Large-Area Planar Wavelength-Extended InGaAs p-i-n Photodiodes Using Rapid Thermal Diffusion With Spin-On Dopant Technique

Chi-Chen Huang, Chong-Long Ho, and Meng-Chyi Wu

***Abstract*— In this letter, we report the large-area planar-type 2.2-μm wavelength-extended InAsP/InGaAs/InAsP p-i-n photodetectors (PDs) using the rapid thermal diffusion (RTD) technique. The zinc-phosphorous-dopant-coating was used as the spin-on dopant source, which was driven into the InAsP/InGaAs heterostructure to form the p-type cap layer of p-i-n diode through the RTD process. The Si/Al_2O_3 bilayers were deposited as the antireflective coating to improve the responsivity of vertically illuminated the PDs. The 800-μm-diameter PD exhibits a low dark current of 4.1 $\times$ 10^{-8} A (8.2 $\times$ 10^{-6} A/cm^2) at -10 mV, a cutoff wavelength of 2.2 μm, a quantum efficiency of above 90% in the wavelength range of 1.4–2.0 μm, and a high responsivity of 1.45 A/W at 2-μm wavelength at room temperature. In addition, the PD exhibits good uniformity in the light received area in the illuminated power range of 0.1–2.0 mW.**

***Index Terms*— p-i-n photodiodes, wavelength-extended, rapid thermal diffusion (RTD), spin-on-dopant (SOD), zinc-phosphorous-dopant-coating (ZPDC).**

I. Introduction

The cutoff wavelength-extended InGaAs photodetectors (PDs) have been widely applied to night vision, remote sensing, environmental research, weather forecast, plastic recycling, pharmaceutical quality inspection, etc. The cutoff wavelength of $In_xGa_{1-x}As$ PDs can be extended from 1.7 to 2.2 μm at room temperature by increasing the indium content from 53% to 73%, which corresponds to bandgap shrinkage from 0.74 eV to 0.56 eV [1]. In contrast to the well known 1.7-μm InGaAs PDs, the 2.2-μm InGaAs PDs suffer from the excessive dark leakage due to high misfit dislocation density generated by 1% lattice mismatch between the $In_{0.73}Ga_{0.27}As$ active layer and the InP substrate. In order to accommodate the lattice mismatch between $In_xGa_{1-x}As$ active layer and the InP substrate, the InGaAs, InAsP, and AlInAs alloys are usually grown as the graded-composition buffer layers for the wavelength-extended InGaAs PDs [2]–[4].

The wavelength-extended InGaAs PDs usually have a structure of p-i-n, which has some advantages of simple manufacturing process and extremely low leakage current. D'Hondt *et al.* reported that the fabricated mesa-type wavelength-extended InGaAs PD with a 600 $\times$ 600 μm^2 window has a dark current of 62 μA at 300K and -10 mV, which is higher than the planar-type one of 32 μA (8.9 $\times$ 10^{-3} A/cm^2) [2]. Zhang *et al.* reported InGaAs PDs with a cutoff wavelength of 2.2 and 2.5 μm at 290 K and -10 mV have a dark current of 57 nA (7.3 $\times$ 10^{-4} A/cm^2) and 67 nA (8.9 $\times$ 10^{-4} A/cm^2), respectively [3]. Cao *et al.* reported the mesa-type InGaAs/InAsP PDs with extending the wavelength to 2.43 μm have a dark current density of 1.37 $\times$ 10^{-5} A/cm^2 at 200K and -10 mV [4]. However, such devices still reveal a relatively high dark current density in the range of 10^{-4}-10^{-3} A/cm^2 at a bias of -10 mV and room temperature.

As compared to the mesa-type PDs, the planar-type PDs always exhibit a low leakage current and long-term stability [5]. For the planar-type InGaAs PDs, the p-type cap layer was usually performed by post-growth zinc-diffusion using the furnace diffusion with zinc arsenide (Zn_3As_2) source [6] and metalorganic vapor phase diffusion (MOVPD) with dimethylzinc (DMZ) or diethylzinc (DEZ) source [7]. However, the furnace diffusion has some disadvantages, including the lack of lateral uniformity and reproducibility, and the restriction of wafer size. The MOVPD can improve the drawbacks of the furnace diffusion, but its cost is too high.

In this letter, we fabricate the large-area planar-type InAsP/InGaAs/InAsP heterostructure p-i-n PDs with a cutoff-wavelength extended to 2.2 μm by rapid thermal diffusion (RTD).

II. Experimental

The epitaxial layers were grown on the S-doped (100) n^+-InP substrate by MOCVD using metamorphic epitaxial growth technique with a compositionally $InAs_yP_{1-y}$ graded buffer layer to mitigate the 1% lattice mismatch between the $In_{0.73}Ga_{0.27}As$ active layer and the InP substrate. The epitaxial device structure of PD consists of a 3-μm n^--$InAs_yP_{1-y}$ (y = 0-0.41) graded buffer layer, a 3-μm n^--$InAs_{0.41}P_{0.59}$ buffer layer, a 3.5-μm n^--$In_{0.73}Ga_{0.27}As$ absorption layer, and a 0.55-μm n^--$InAs_{0.41}P_{0.59}$ cap layer.

For planar-type InGaAs p-i-n PDs, the p-type cap layer was performed by selective-area zinc-diffusion technique. A SiO_2 layer was deposited onto the surface by plasma-enhanced chemical vapor deposition (PECVD), and then 800-μm-diameter windows were formed by dry etching for the following zinc driven-in process as diffusion masks. The zinc driven-in process was performed by RTD with spin-on-dopant (SOD) technique [8]. The zinc-phosphorous-dopant-coating (ZPDC) was first spun onto a 2-inch sapphire wafer as a zinc source-carreir. A semi-closed chamber was then formed by a source-carreir capped onto the PD-wafer.

Manuscript received May 5, 2015; revised May 29, 2015; accepted June 11, 2015. Date of publication June 15, 2015; date of current version July 22, 2015. This work was supported by the National Science Council under Grant 103-2218-E-007-002- and Grant 103-2622-E-007-009-CC2. The review of this letter was arranged by Editor D. H. Kim. *(Corresponding author: Meng-Chyi Wu.)*

The authors are with the Institute of Electronics Engineering, National Tsing Hua University, Hsinchu 30013, Taiwan (e-mail: mcwu@ee.nthu.edu.tw).

Color versions of one or more of the figures in this letter are available online at http://ieeexplore.ieee.org.

Digital Object Identifier 10.1109/LED.2015.2445471

0741-3106 © 2015 IEEE. Personal use is permitted, but republication/redistribution requires IEEE permission.
See http://www.ieee.org/publications_standards/publications/rights/index.html for more information.

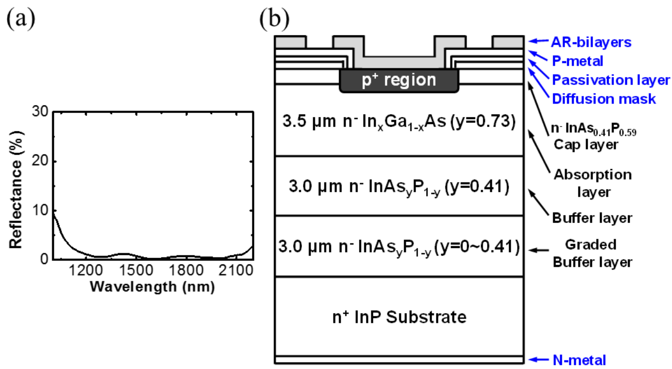

Fig. 1. (a) Reflectance of Si/Al_2O_3 anti-reflection (AR) coating as a function of wavelength. (b) Schematic cross-section of planar InGaAs p-i-n PDs.

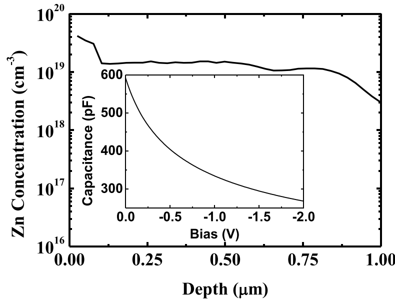

Fig. 2. Depth profile of Zn dopant driven into the InGaAs PDs by SIMS analyses. Inset: Capacitance versus reverse-bias curves of PDs measured at 298 K.

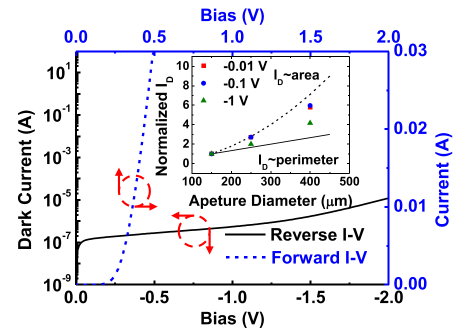

Fig. 3. Typical current versus forward and reverse bias curves of PDs measured at 298K and in dark. Inset: Normalized dark current as a function of aperture diameter of PDs measured at 298K.

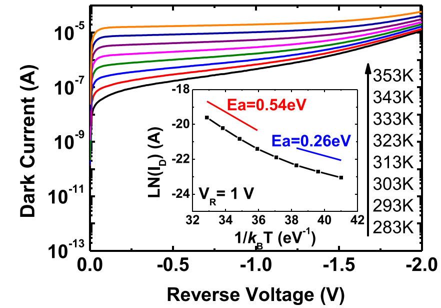

Fig. 4. Temperature dependence of I-V characteristics for the PDs. Inset: Activation energy extracted from the dark-current characteristics at −1 V in the temperature range of 283-353K.

The zinc driven-in process was subsequently done by RTD in nitrogen (N_2) ambience and followed by acceptor activation. In order to inhibit the phosphorus loss from the $InAs_{0.41}P_{0.59}$ cap layer, the zinc driven-in process using ZPDC as zinc source was performed at a relatively low temperature of 400°C, followed by an activation treatment at 450°C. Afterwards, the p-end illuminated devices were fabricated as the following SiO_2 dielectric passivation, p-metal Cr/AuZn/Au alloy deposition, and 150-nm Si/250-nm Al_2O_3 anti-refletion (AR) coating deposition. The reflectance of AR coating is lower than 3% in the wavelength range of 1.2-2.2 μm, as shown in Fig. 1(a). After bond-pad metallization, wafer was lapped and polished down to about 200 μm, and then n-metal AuGe/Au alloy was deposited onto the back side of InP substrate. Finally, the wafer was diced into chips with a size of 1.2 mm × 1.2 mm and then mounted onto the transistor outline (TO) header. The schematic structure of InAsP/InGaAs/InAsP planar p-i-n PDs with a cutoff-wavelength extending to 2.2 μm is shown in Fig. 1(b).

III. Results and Discussion

Fig. 2 shows the depth profile of zinc in the diodes measured by secondary ion mass spectrometer (SIMS). The analysis reveals that the zinc dopants can be driven-in through the 0.55-μm InAsP cap layer into InGaAs active layer to form a p-n junction by RTD with ZPDC source. The zinc concentration is above 1×10^{19} cm^{-3} in InAsP cap layer. Inset shows the typical capactitance as a function of reverse bias (C-V) curves of PDs measured at 298K in dark for the PDs. The PDs have a capacitance of 330 pF at −5 V and the deduced concertation of InGaAs active layer is about 5×10^{16} cm^{-3}.

Fig. 3 shows the typical current as a function of forward and reverse biases (I-V) characteristics of PDs measured at 298K in dark. The device has a turn-on voltage of 0.3 V and a series resistance of 10 Ω at an injection current density of 1 A/cm^2, and a specific shunt resistance of 181 Ω-cm^2. The PDs exhibit a low dark current of 4.1×10^{-8} A (8.2×10^{-6} A/cm^2) at −10 mV, and 5.4×10^{-7} A (1.1×10^{-4} A/cm^2) at −1 V. The dark current density of the PDs is lower than those reported of 1.3×10^{-5} A/cm^2 at 274K and −0.1 V for the 2.1-μm PD with a 1-mm-diameter window [9], 7.3×10^{-4} A/cm^{2}at 290K and −10 mV for the 2.2-μm PD with a 100-μm-diameter window [3], and 5×10^{-5} A/cm^2 at 293K and −10 mV for the 2.4-μm PD [10]. To investigate the dominant source of dark current, the normalized dark current versus aperture diameter of PD at 298K is shown in the inset of Fig. 3. The results indicate that the dark current is dominated by the bulk-area current at lower biases, while it is attributed to the surface-perimeter current at higher biases [2].

Fig. 4 shows the typical dark current versus reverse bias characteristics of PDs in the temperature range from 283 to 353K with 10K/step. At a bias of −10 mV, the dark current of the PD is 4.2 μA at 353K, and decreases to 9.4 nA (1.9×10^{-6} A/cm^2) at 283K. The inset shows the activation energy (E_a) calculated from the dark current at -1 V in the temperature range of 283-353K. The extracted E_a of the PD are 0.54 and 0.26 eV at about 353 and 283K, respectively. These values approximately agree with the bandgap (E_g) and $E_g/2$ of $In_{0.73}Ga_{0.27}As$ absorption region, respectively. Therefore, the dark current of PD is dominated by diffusion current at higher temperatures and generation-recombination current at lower temperatures.

Fig. 5 shows the three-dimension photoresponse uniformity of PDs measured at room temperature and zero bias. The

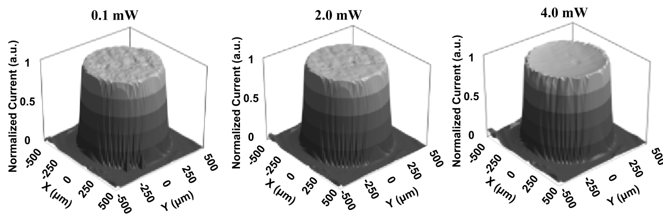

Fig. 5. Plots of three-dimension photoresponse profiles for PDs with different illuminated powers at zero bias and room temperature.

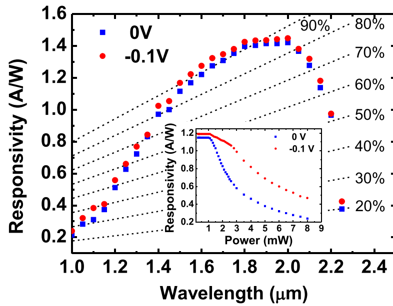

Fig. 6. Response spectra of PDs measured under the ~1-μW illumination power at room temperature and biases of 0 and −0.1 V. Inset: Responsivity of PDs versus optical power of 1.55-μm wavelength measured at room temperature and biases of 0 and -0.1 V.

PD was perpendicularly illuminated by a 1.55-μm laser beam with the illumination power range of 0.1-4.0 mW through a single fiber, and the light-received area of PD was scanned with 25-μm scan per step. The results reveal that the photoresponse is uniform across the large-area PDs in the illumination power range of 0.1-2.0 mW, while the responsivity of detector is varied with the spot position at the high illumination power of 4.0 mW. The photo-current shows uniform across the large-area PDs under the low illumination powers, which could mean that the p-n junctions are uniformly formed by using RTD with SOD technique. The photo-current uniformity exhibits slightly concave at the light-received center under the high illumination power, which is called the current (carrier) crowding effect. It is attributed to that the lateral resistance of the p-$InAs_{0.41}P_{0.59}$ contact layer would prevent the photo-generated carriers from being instantaneously received, especially under high illuminated powers.

Fig. 6 shows the responsivity spectra of PDs measured at room temperature and the biases of 0 and −0.1 V. At room temperature, the sharp cutoff-wavelength at 2.2 μm is ascribed to the the bandgap of $In_{0.73}Ga_{0.27}As$ absorption layer, while the efficiency decay at the spectral range below 1.4 μm is caused by the absorption in the p-type $InAs_{0.41}P_{0.59}$ cap layer with a bandgap of 0.87 eV (or 1.425 um). The detector have a responsivity of 1.42 A/W and a quantum efficiency of 88% at 2.0-μm wavelength at zero bias. At an applied bias of −0.1 V, a responsivity and a quantum efficiency can enhance to 1.45 A/W and 90% at 2.0-μm wavelength, respectively. This peak responsivity of 1.45 A/W at 2.0 μm is higher than that of 1.14 A/W at 1.7 μm [4]. The quantum efficiency in the 1.4-2.0 μm range is over 85% at 0 V and over 90% at −0.1 V, which is comparable to or better than the reported values of 80-90% [9], and 70% at 2.1 μm [3]. The high responsivity and quantum efficiency of PDs can be attributed to the use of planar device structure, Si/Al_2O_3 AR-coating, and RTD with ZPDC-SOD technique. Inset shows the optical power dependencies of the responsivity at 1.55-μm wavelength of PDs biased at 0 and -0.1 V. Due to charge screening effect, the responsivity drops as the power increases [11]. The saturation powers at 0 and -0.1 V, which are defined at the 1% decay of the responsivity compared to the low-power value, are 1.1 and 1.2 mW, respectively.

IV. Conclusions

We have successfully fabricated the large-area planar-type InAsP/InGaAs/InAsP heterostructure p-i-n PDs with a cutoff-wavelength extending up to 2.2 μm by RTD with ZPDC-SOD method. The device exhibits a low dark current of 4.1×10^{-8} A (8.2×10^{-6} A/cm^2) and 5.4×10^{-7} A (1.1×10^{-4} A/cm^2) at −10 mV and −1 V, respectively. The Si/Al_2O_3 AR-bilayers, which reduce the surface reflectance to be lower than 3%, are used to improve the incident light coupling and to enhance the responsivity of vertically illuminated PDs. In the wavelength range of 1.4-2.0 μm, the PD has a high quantum efficiency of above 90%. The PD exhibits a cutoff -wavelength of 2.2 μm, a high responsivity of 1.45 A/W at 2.0-μm wavelength. Furthermore, the PD has good uniformity in the light received area in the illuminated power range of 0.1-2.0 mW. The results illustrate that the large-area planar-type 2.2-μm wavelength-extended InGaAs p-i-n PDs can be well developed by RTD with ZPDC-SOD technique.

References

[1] K. R. Linga *et al.*, "Dark current analysis and characterization of $In_xGa_{1-x}As/InAs_yP_{1-y}$ graded photodiodes with x > 0.53 for response to longer wavelengths (>1.7 μm)," *J. Lightw. Technol.*, vol. 10, no. 8, pp. 1050–1055, Aug. 1992.

[2] M. D'Hondt *et al.*, "Influence of buffer layer and processing on the dark current of 2.5 μm-wavelength 2%-mismatched InGaAs photodetectors," *IEE Proc.-Optoelectron.*, vol. 144, no. 5, pp. 277–282, Oct. 1997.

[3] Y. Zhang *et al.*, "Gas source MBE grown wavelength extended 2.2 and 2.5 μm InGaAs PIN photodetectors," *Infr. Phys. Technol.*, vol. 47, no. 3, pp. 257–262, Jan. 2006.

[4] G. Cao *et al.*, "Performance of extended wavelength InGaAs/InAsP SWIR detector," *Proc. SPIE*, vol. 9284, pp. 928406-1–928406-8, Sep. 2014.

[5] C. P. Skrimshire *et al.*, "Reliability of mesa and planar InGaAs PIN photodiodes," *IEE Proc. J. Optoelectron.*, vol. 137, no. 1, pp. 74–78, Feb. 1990.

[6] M. H. Ettenberg *et al.*, "Zinc diffusion in InAsP/InGaAs heterostructures," *J. Electron. Mater.*, vol. 28, no. 12, pp. 1433–1439, 1999.

[7] M. Wada, K. Izumi, and K. Sakakibara, "Diffusion of zinc acceptors in InAsP by the metal-organic vapor-phase diffusion technique," *Appl. Phys. Lett.*, vol. 71, no. 7, pp. 900–902, Jun. 1997.

[8] C.-C. Huang *et al.*, "Large-area planar InGaAs p-i-n photodiodes with Mg driven-in by rapid thermal diffusion," *IEEE Electron Device Lett.*, vol. 35, no. 12, pp. 1278–1280, Dec. 2014.

[9] M. Wada and H. Hosomatsu, "Wide wavelength and low dark current lattice-mismatched InGaAs/InAsP photodiodes grown by metalorganic vapor-phase epitaxy," *Appl. Phys. Lett.*, vol. 64, no. 10, pp. 1265–1267, Mar. 1994.

[10] X. Ji *et al.*, "Deep-level traps induced dark currents in extended wavelength $In_xGa_{1-x}As/InP$ photodetector," *J. Appl. Phys.*, vol. 22, no. 114, pp. 224502-1–224502-5, Dec. 2013.

[11] J. Harari *et al.*, "Modeling of waveguide PIN photodetectors under very high optical power," *IEEE Trans. Microw. Theory Techn.*, vol. 43, no. 9, pp. 2304–2310, Sep. 1995.